Effect of Lattice Relaxation on Cation Exchange in Zeolite A Using Computer Simulation

F. Manon Higgins,* Graeme W. Watson, and Stephen C. Parker†

Computational Solid State Chemistry Group, School of Chemistry, University of Bath, Claverton Down, Bath BA2 7AY, United Kingdom

Received: May 30, 1997; In Final Form: August 18, 1997[⊗]

Atomistic simulation techniques based on the Born model of ionic solids have been used to investigate adsorption and ion exchange of Ba^{2+}, Sr^{2+}, Ca^{2+}, Cd^{2+}, Ni^{2+}, Co^{2+}, Cs^{+}, K^{+}, and Na^{+} in dehydrated zeolite A. This work has shown that relaxation of the framework greatly affects the position of the most stable exchangeable cation sites. The results have considerable consequences for simulation studies showing that simulations are meaningful only if the framework is allowed to relax freely. The aluminum content in the zeolite framework was found to influence the size of the ring structures, which in addition influences the exchangeable cation positions. The simulation results have identified stable adsorption sites for the exchangeable cations, which show good agreement with experimental crystallographic data. This indicates the viability of using atomistic simulation to probe the structure, stability, and diffusivity in zeolites.

1. Introduction

Heavy metals and radionuclides are both hazardous cationic species, and their interaction with soils has received increasing attention in recent years.[1] Ion exchange is regarded as one of the key processes that regulate the mobility of these hazardous species within the environment, but it can also be the process used for the decontamination of polluted soil, (ground)water or effluent. An ion exchanger, often a zeolite, which is specific to the type of contamination, can be used selectively to remove it. For example, clinoptilolite has been used to remove cesium and strontium from radioactively contaminated soil.[2,3] Phillipsite has been used to remove cadmium from acid mine drainage,[4] and synthetic zeolites such as faujasites X and Y have been used to adsorb cobalt and nickel to treat nuclear aqueous waste.[5] Zeolites can also be used for long-term storage of long-lived radioisotopes by drying the zeolite and sealing in a container for burial. As the zeolites are highly selective toward the radioisotopes, they concentrate and therefore reduce the radioactive waste volume. At elevated temperatures the contamination-saturated zeolite can be converted to glass, which has an extremely low leach rate.[6]

For these reasons we decided to model cation-exchange and adsorption behavior in common simple zeolite structures. Dehydrated zeolite A was chosen as a model structure to test these simulation techniques as there are available experimental crystallographic data with which to compare and to allow us to verify the methodology we are developing. Previous single-crystal X-ray diffraction experiments have identified cation adsorption sites, e.g. for potassium,[7,8] cesium,[9,10] and cadmium[11] in dehydrated zeolite A. In addition, atomistic calculations have been used successfully before to study structural and reactivity properties for a range of zeolites, including sodium-exchanged zeolite A.[12−14] The stability of a range of exchangeable cations was investigated in three dehydrated zeolite A type structures, (i) the siliceous form (where the aluminum(s) and charge-compensating cation, either sodium or calcium, are at infinite dilution), (ii) with Si/Al = 1, fully charge compensated with Ca/Na = 1 (referred to as CaNa-A), and (iii) with Si/Al = 1 and Ca/Na = 2.5 (referred to as Ca_5Na_2-A). The choice of exchangeable cations studied was based on two criteria: (1) their environmental importance, either as a natural charge-compensating cation or potential pollutant, and (2) their varied ionic radii. (For brevity we shall refer to the exchangeable cations as cations, and when we need to refer to the framework cations, i.e., silicon and aluminum, we mention them explicitly.)

2. Theoretical Methodology and Potentials

2.1. Theory. The simulation methods are based upon energy minimization calculations according to the Born model of ionic solids[15] in which the forces between the atoms are described by interatomic potentials (section 2.2). We chose this approach rather than a full quantum mechanical treatment because the size of the simulated cell and the number of simulations would be prohibitive and furthermore, as noted earlier, this approach has been very successfully applied to modeling zeolites.

Energy minimization simulations were performed on the bulk of the dehydrated zeolite A structures prior to considering cation adsorption and exchange using three-dimensional periodicity with the reduced unit cell (for computation ease) with the computer code PARAPOCS.[16] The siliceous and the 1:1 Si/Al ratio cells with the two Ca/Na distributions were relaxed to their minimum energy structure to provide a reliable starting configuration for further stages of our study. Provided that there is good agreement with available crystallographic data, the next step is to calculate the defect energies of the exchangeable cations at various possible locations in the zeolite lattices to identify stable cation adsorption sites. However, a limitation of the energy minimization methods is that they cannot be guaranteed to locate the global minimum energy site if the ion needs to pass an energy barrier from the starting configuration. This may be overcome by either using Monte Carlo or molecular dynamics simulations or simply starting the simulations from all plausible starting points.

We chose to obtain reasonable starting positions for the cations in our simulations by performing a grid scan within the whole unit cell. A single calcium or sodium cation is moved to different points on a grid in 0.023 Å steps through the purely siliceous, energy-minimized zeolite A structure. At each point the interaction energy is calculated and a potential energy surface is obtained. Reasonable cation starting positions can be identified by examination of this potential energy surface employing a simple statistical thermodynamic treatment (using a Boltzmann distribution) to predict occupancy at each point at elevated temperatures.

Once the probable cation positions are identified, defect calculations are performed within the CASCADE[17] program.

* Corresponding author. Tel: 01225-826523. Fax: 01225-826231. Email: chpfmb@bath.ac.uk. URL: http://www.bath.ac.uk/∼chsscp/group/.
† Email: s.c.parker@bath.ac.uk.
⊗ Abstract published in *Advance ACS Abstracts,* October 15, 1997.

S1089-5647(97)01752-5 CCC: $14.00

This compares the minimum energy of the nondefective lattice with the relaxed defective lattice. The approach is to use a two-region strategy, by defining a spherical region (region I) around the defect, which is explicitly relaxed. In our case this region holds typically 200−250 ions and has a cutoff size set to 10.0 Å to ensure convergence. This is surrounded by region II comprising typically 4000−6000 ions, and the remainder of the crystal is modeled using a quasi-continuum approximation.[18] The methodology behind the CASCADE program is reviewed extensively elsewhere.[19] Previous work has shown that, provided one uses a sufficiently large inner region, the CASCADE program, in combination with reliable interatomic potentials, can produce accurate values of the energies of ion adsorption, substitution, and migration.[20−22]

2.2. Potentials. There are now many potential models in the literature (see, for example, reviews by Lewis and Catlow[23] or Gale[24]). These are tested by checking the agreement with experimental data, such as crystal structure and elastic constants. The two-body component of the potential model used in our simulations for the interaction of ions i and j at a distance of r_{ij} is given by an analytical expression of the form:

$$\Phi_{ij}(r_{ij}) = \frac{-Z_i Z_j e^2}{r_{ij}} + A_{ij}\exp\left(\frac{-r_{ij}}{\rho_{ij}}\right) - \frac{C_{ij}}{r_{ij}^6}$$

where Z_i and Z_j are the charges on the ions i and j and A_{ij}, ρ_{ij}, and C_{ij} are potential model parameters that are commonly fitted to experimental data (empirical fitting) or to electronic structure calculations (nonempirical fitting). The first term of the equation corresponds to the long-range Coulombic interaction. The second term is meant to represent the repulsive forces at small distances (due to overlap of electron clouds), and the third attractive term represents van der Waals interactions.

As charged defects can polarize other ions in the crystal, ionic polarizability must be incorporated into the potential model. Dick and Overhauser's shell model[25] is a very simple but effective mechanical model, which considers each polarizable ion (in our case oxygen) to consist of a core (representing the nucleus and core electrons) and a massless shell (representing the valence electrons), connected by a harmonic spring. The polarizability of the model ion is then determined by the spring constant and the charges of the core and shell. These are usually obtained by empirical fitting to the dielectric properties of the crystal, when available.[26]

A range of potentials were used, those that were found to be most appropriate are given in Table 1b, section I, while other potentials tested are shown in Table 1b, section II. Additional information required for the potential models are tabulated in Table 1a,c. We used the fully ionic model derived empirically by Sanders et al.[27] for the silica framework, that incorporates the O−O interaction derived from electronic structure calculations, because it has been shown to be highly transferable[23,28,29] and thus reduces the need for additional derivation of potential models for each new cation introduced to the zeolite crystal. Additionally, due to the paucity of appropriate experimental data for the alkali oxides, we used potentials derived by a different approach, namely, the nonempirical modified electron gas method (MEG)[35] for sodium, potassium, and cesium. The suitability of the potentials was tested by comparison with the experimental structural (Table 2a) and elastic tensor data (Table 2b) of a range of alkali and alkaline earth aluminosilicates. The combination of the potentials shown in Table 1b, section I, gives the best reproduction for the minerals investigated as is clearly shown by the percent difference between experiment and calculation in Table 2a. However, the results were not as conclusive with regard to the calcium potential, and we therefore chose to use both potentials in this zeolite study (section 6 only). In addition, we have also included a second strontium potential to enable us to assess the sensitivity of the simulation results to the potential model used (section 6).

TABLE 1: Potential Parameters Based on the Three-Body Shell Model Potential of Sanders et al., 1984[27]

(a) Charges and Masses

species	charge (e)	mass (g mol^{-1})	species	charge (e)	mass (g mol^{-1})
O_{core}	0.86902	15.9994	Cd	2.0	112.40
O_{shell}	−2.86902	0.00	Ni	2.0	58.71
Si	4.0	28.0855	Co	2.0	58.9332
Al	3.0	26.9815	Cs	1.0	137.00
Ba	2.0	137.34	K	1.0	39.0983
Sr	2.0	90.00	Na	1.0	22.9898
Ca	2.0	40.08			

(b) Buckingham Potential Parameters[a] (Short-Range Cutoff: 18.5 Å)

interaction	Å/eV	ρ/Å	C/eV Å^6	method	ref
Section I					
O−O	22764.000	0.1490	27.88	HF	33, 30
Si−O	1283.907	0.32053	10.66158	EMP	27
Al−O (Al1)	1460.300	0.29912	0.0	EMP	30
Ba−O	905.700	0.3976	0.0	EMP	23
Sr−O (Sr1)	959.100	0.3721	0.0	EMP	23
Ca−O (Ca1)	1090.400	0.3437	0.0	EMP	23
Cd−O	1064.900	0.3389	0.0	EMP	this work
Ni−O	1582.500	0.2882	0.0	EMP	23
Co−O	1491.700	0.2951	0.0	EMP	23
Cs−O	1065.320	0.3911	0.0	MEG	32
K−O (K2)	65269.710	0.2134	0.0	MEG	31
Na−O (Na2)	5836.814	0.2387	0.0	MEG	31
Section II					
Al−O (Al2)	1012.600	0.3118	0.0	MEG	23
Sr−O (Sr2)	1299.280	0.3635	0.0	MEG	32
Ca−O (Ca2)	6958.230	0.2515	0.0	MEG	31
K−O (K1)	1000.300	0.36186	0.0	EMP	34
Na−O (Na1)	1266.840	0.3840	0.0	EMP	32

(c) Shell Model and Three-Body Force Constants

interaction	force constant	ref
$O_{core}-O_{shell}$	74.92 eV Å^{-2}	27
$O_{shell}-Si-O_{shell}$	2.09724 eV rad^{-2}	27
$O_{shell}-Al-O_{shell}$	2.09724 eV rad^{-2}	28

[a] Parameters in section I are the preferred parameters. [b] Derivation methods: HF, Hartree−Fock; EMP, empirical; MEG, modified electron gas.

3. Crystal Structure

The crystallographic structure of zeolite A may be described as an octahedral array of sodalite units. These sodalite units, or β-cages, consist of six four-membered rings (4R) separated by eight adjoining six-membered rings (S6R).[43,44] By arranging the β-cages at the corners of a cube, linking them in double four-membered rings (D4R), the zeolite framework is obtained. This cubic structure creates large α-cages separated by single eight-membered rings (S8R) on the face of the cube (see Figure 1).[45] Extending the zeolite framework in the x, y, and z directions creates a three-dimensional network of channels, giving rise to the molecular sieve character.[44,46]

Three crystallographically different oxygen sites are observed in the zeolite A structure O(1), O(2) and O(3). In the β-cage, the oxygens that build up the four-rings consist of O(3), while the six-rings are built up from both O(2) and O(3). The O(1) oxygens form the bridges between the adjacent sodalite units (see Figure 1).[45] The framework is stoichiometric with a Si/Al ratio of 1, which gives rise to a net negatively charged unit cell ($[Si_{24}Al_{24}O_{96}]^{-24}$) that needs to be compensated by exchangeable cations, which are located in specific adsorption sites inside the zeolite framework.[44,46]

TABLE 2: Potential Parameters Tested for Their Transferability to a Range of Experimental Alkali and Alkaline Earth Aluminosilicate Structures

(a) Comparison of Lattice Vectors (% difference) and Angles

potential	*a* (Å)	*b* (Å)	*c* (Å)	α	*β*	*γ*	volume (Å)
			α-Quartz (SiO_2)				
exptl[36]	4.91	4.91	5.40	90.00	90.00	120.00	113.01
3-body	4.89 (−0.4)	4.89 (−0.4)	5.40 (+0.0)	90.00	90.00	120.00	111.61 (−1.2)
			Albite ($NaAlSi_3O_8$)				
exptl[37]	8.14	12.79	7.16	94.27	116.60	87.69	663.9
3b Na1 Al1	8.49 (+4.4)	12.91 (+1.0)	7.16 (+0.0)	91.42	115.98	87.87	705.49 (+6.2)
3b Na1 Al2	8.42 (+3.4)	12.77 (−0.1)	7.06 (−1.3)	91.92	116.09	88.95	681.37 (+2.5)
3b Na2 Al1	8.18 (+0.5)	12.77 (−0.1)	7.08 (−0.1)	93.64	116.54	88.00	660.67 (−0.6)
3b Na2 Al2	8.11 (−0.4)	12.64 (−1.1)	6.98 (−2.4)	93.63	116.76	89.15	637.57 (−4.1)
			Diopside ($CaMgSi_2O_6$)				
exptl[38]	9.75	8.92	5.25	90.00	105.86	90.00	439.13
3b Ca1	9.81 (+0.7)	9.06 (+1.5)	5.28 (+0.5)	90.00	105.44	90.00	452.08 (+3.0)
3b Ca2	9.57 (+1.8)	8.73 (−2.1)	5.20 (−0.9)	90.00	104.84	90.00	420.34 (−4.3)
			Microcline ($KAlSi_3O_8$)				
exptl[39]	8.58	12.96	7.22	90.68	115.94	87.65	721.30
3b K1 Al1	9.18 (+7.0)	12.84 (−1.0)	7.27 (+0.9)	90.41	115.18	88.27	774.33 (+7.4)
3b K1 Al2	9.13 (+6.5)	12.67 (−2.3)	7.17 (−0.7)	90.47	115.28	89.00	750.11 (+4.0)
3b K2 Al1	8.61 (+0.4)	12.91 (−0.4)	7.15 (−0.9)	90.41	115.93	87.87	714.43 (−1.0)
3b K2 Al2	8.54 (−0.4)	12.76 (−1.5)	7.06 (−2.2)	90.82	115.99	88.89	692.04 (−4.1)

(b) Comparison of Experimental and Calculated Elastic Constants[28]

	elastic constants in GPa									
potential	C_{11}	C_{22}	C_{33}	C_{44}	C_{55}	C_{66}	C_{12}	C_{13}	C_{23}	K_s
					α-Quartz (SiO_2)					
exptl[40]	87	87	106	58	58	40	7	12	12	37
3-body	96	96	112	51	51	42	13	17	17	44
					Albite ($NaAlSi_3O_8$)					
exptl[41]	74	131	128	17	30	32	36	39	31	
3b Na1 Al1	74	192	149	12	37	45	46	38	20	56
3b Na1 Al2	77	200	156	18	40	47	47	41	23	58
3b Na2 Al1	89	194	159	23	39	44	48	44	19	64
3b Na2 Al2	94	211	166	28	42	46	50	49	25	67
					Diopside ($CaMgSi_2O_6$)					
exptl[42]	223	171	235	74	67	66	77	81	57	108
3b Ca1	220	168	245	67	68	69	91	90	67	117
3b Ca2	255	188	266	61	71	89	112	98	71	119
					Microcline ($KAlSi_3O_8$)					
exptl[41]	66	171	122	14	24	36	44	26	19	
3b K1 Al1	112	173	149	25	34	47	92	42	26	63
3b K1 Al2	121	175	156	26	36	49	98	44	27	67
3b K2 Al1	99	208	154	20	39	48	70	48	29	74
3b K2 Al2	104	214	164	24	42	48	73	53	32	79

Our initial zeolite A configuration was simulated starting from crystallographic data of a commercial dehydrated zeolite 5A.[47] The crystallographic structure was determined by neutron powder diffraction techniques in the cubic space group $Fm\bar{3}c$, (a = 24.6497(8) Å) with two unique cation adsorption sites. Both the calcium and sodium species are located near the six-ring windows; however, the sodium atoms are located inside the α-cage, while the calcium sites are inside the sodalite units. The final structural composition was $Ca_{40}Na_{16}Si_{96}Al_{96}O_{384}$ with a Si/Al ratio of 1.02 . We minimized this structure in a purely siliceous form to constant pressure. The unit cell volume of the minimized structure had decreased by 12.6%. This reduction in volume was expected since the experimental structure contained aluminum in its framework and charge-compensating cations.

4. Cation Exchange and Adsorption in Siliceous Zeolite A

4.1. Effect of Framework. Initial calculations of the cation sites were performed by a three-dimensional grid scan of a single calcium or sodium cation through the above-mentioned siliceous structure, while keeping the framework positions fixed. The interaction energy between cation and lattice was calculated, and from these interaction energies the relative probability distributions were obtained using a simple statistical mechanical treatment (as described in section 2.1).

At 300 K the highest site probability was found to be in the center of the eight- rings (S8R) for both the cation species (corresponding to interaction energies of −3.74 eV for Ca and −2.04 eV for Na). By increasing the temperature to 1500 K, another possible adsorption site with a lower probability appeared corresponding to the six-ring sites (S6R) (with interaction energies of −3.25 eV for Ca and −1.67 eV for Na). These findings disagree with the crystallographic data by Adams and Haselden[47] and Vance and Seff,[9] who identified the six-rings as the adsorption sites where calcium and sodium are located. The difference between our results and experiment might be due to the absence of aluminum in the zeolite lattice, which would compensate for the repulsive forces between the silicon atoms in the framework and the cation (as the aluminum atoms in the framework are effectively negatively charged). Additionally, the effect of lattice relaxation on the energy and position of the cation is not taken into account as the lattice was kept rigid. In section 5 we study the effect of aluminum

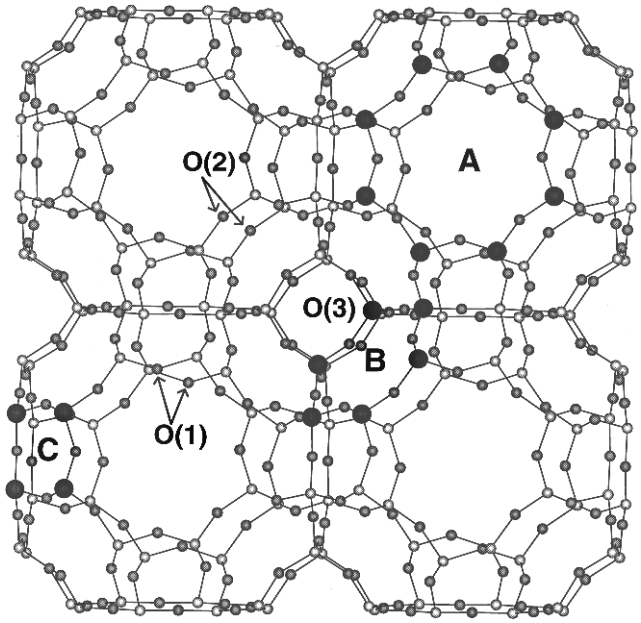

Figure 1. Siliceous structure of dehydrated zeolite A, where the eight-ring (A), six-ring (B), and four-ring (C) are shown in bold, and where O(1), O(2), and O(3) are also identified.

TABLE 3: List of Cations Used in the Atomistic Calculations, Along with Their Environmental Importance

exchangeable cations		
common cations	heavy metals	radionuclides
Ba^{2+}, Ca^{2+}, K^{+}, Na^{+}	Cd^{2+}, Co^{2+}, Ni^{2+}	Co−60, Cs−137, Sr−90

addition to the zeolite framework. However, first we investigate the effect of framework relaxation.

4.2. Framework Relaxation. The scan of a single sodium and calcium cation through the rigid siliceous framework identified plausible starting positions for the energy minimization study of the adsorption stability of a range of exchangeable cations (see Table 3). The two most significant starting positions were the eight-ring window (or S8R site) and six-ring window, where the six-ring was identified in previous X-ray experiments to consist of two possible positions, one just inside the α-cage (the S6R site) and the other just inside the sodalite unit (referred to as the S6R′ site). The results are reported in Table 4, comparing the relative defect energies in both the rigid and relaxed lattice for each cation at the three starting positions. The results shown in bold are the lowest energy configurations in both the rigid and the relaxed zeolite framework. Where two energies are highlighted, we suggest that the energies are the same within error (as the difference in energy is only 0.02 and 0.03 eV).

The most significant result is that framework relaxation is a very important component in the interaction between cation and framework and that the lattice cannot be viewed as a rigid structure through which atoms move. Furthermore, the results show that relaxation of the lattice creates a large decrease in the cation defect energies of approximately 2 eV for the monovalent and 7−9 eV for the divalent cations. The relaxation is significant as it shifts the site preference of the exchangeable cations from the S8R to the S6R position, particularly for the cations with an ionic radius of 1.0 Å or less (Ca^{2+}, Cd^{2+}, Co^{2+}, Ni^{2+}, and Na^{+}). All cations found stable or metastable sites at, or near, the initial three positions, see Table 4, where the displacement from the original position is quoted in angstroms. In general, the cations in the S6R site lie along the [111] direction toward the center of the α-cage. Their distance from the six-ring window is related to the ion size (Table 4) (see

TABLE 4: Effect of Lattice Relaxation on the Cation Position in Siliceous Zeolite A[a]

	Defect Energy of Site (eV)					
	eight-ring		six-ring		β-cage	
cation	rigid	relaxed	rigid	relaxed	rigid	relaxed
Cs^{+}	**−0.76**	**−2.67** (1.42)	2.74	−2.53 (2.13)	**−0.79**	−2.27 (0.04)
K^{+}	**−2.01**	**−3.74** (0.12)	−1.13	−3.39 (1.05)	−1.11	−2.99 (1.16)
Na^{+}	**−2.04**	−3.79 (0.04)	−1.61	**−4.01** (0.56)	−1.11	−3.16 (2.09)
Ba^{2+}	**−2.85**	**−9.36** (0.04)	−0.68	−8.28 (1.39)	−1.89	−7.93 (0.64)
Sr^{2+}	**−3.32**	**−10.11** (0.04)	−0.51	−9.24 (1.07)	−2.06	−8.66 (1.10)
Ca^{2+}	**−3.74**	**−10.65** (0.04)	−2.01	**−10.63** (0.72)	−2.15	−10.02 (1.69)
Cd^{2+}	**−3.80**	−10.75 (0.04)	−2.24	**−11.08** (0.61)	−2.16	−9.44 (1.96)
Ni^{2+}	**−5.24**	−11.19 (0.04)	−3.22	**−14.16** (0.17)	−2.21	−11.88 (2.55)
Co^{2+}	**−4.03**	−11.15 (0.04)	−3.13	**−13.73** (0.19)	−2.21	−11.45 (2.47)

[a] The results shown in bold are the lowest energy configurations in both the rigid and the relaxed zeolite framework; where two energies are highlighted, we suggest that the energies are the same within error. Values in parentheses indicate displacement from original position (Å).

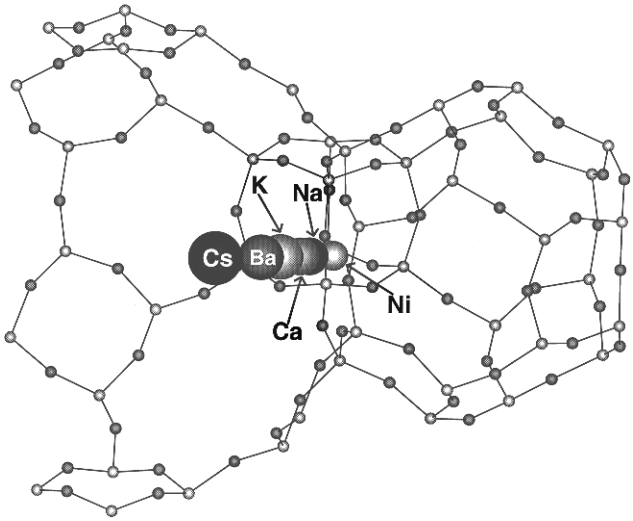

Figure 2. S6R adsorption site: a representation of some of the cation positions near the six-ring window inside the α-cage.

Figure 2). The S6R′ position inside the sodalite unit was only a favored location for the larger cations (Cs^{+}, K^{+}, Ba^{2+}, Sr^{2+}, and Ca^{2+}). Their positions were centered on the six-ring window, along the [111] direction, toward the center of the sodalite unit, with calcium being nearest to the six-ring and cesium remaining in the center of the sodalite unit (see Figure 3). Their distances to the six-ring window are similar to their respective distances inside the α-cage (e.g. 2.13 Å (α-cage) vs 2.14 Å (β-cage) for Cs and 1.17 Å (α-cage) vs 1.21 Å (β-cage) for Sr). The smaller cations inside the sodalite unit (Na^{+}, Cd^{2+}, Co^{2+}, and Ni^{2+}) were located near a four-ring center (4R′ site), with cobalt and nickel moving nearest to the 4R′ oxygens (see Figure 4). The S8R adsorption site was found to be in the plane of the ring and centered, with the exception of cesium, which, although still centered, moved away from the plane of the ring toward the α-cage center (see Figure 5). Another exception was potassium, which moved slightly off-center in the plane of the eight-ring (see Figure 5), which has previously been observed experimentally.[7,8,48]

The cation adsorption sites found in the siliceous zeolite crystal are in agreement with the findings of Ahn and Iton,[49]

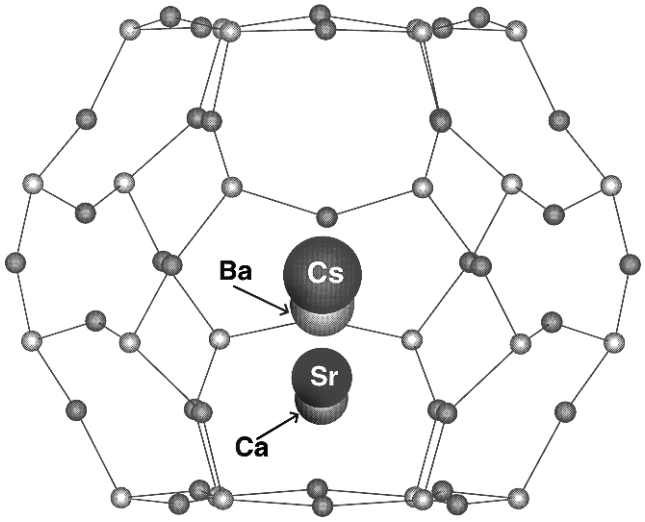

Figure 3. S6R′ adsorption site: a representation of the positions of the larger cations studied, inside the β-cage along the [111] direction toward the hexagonal window.

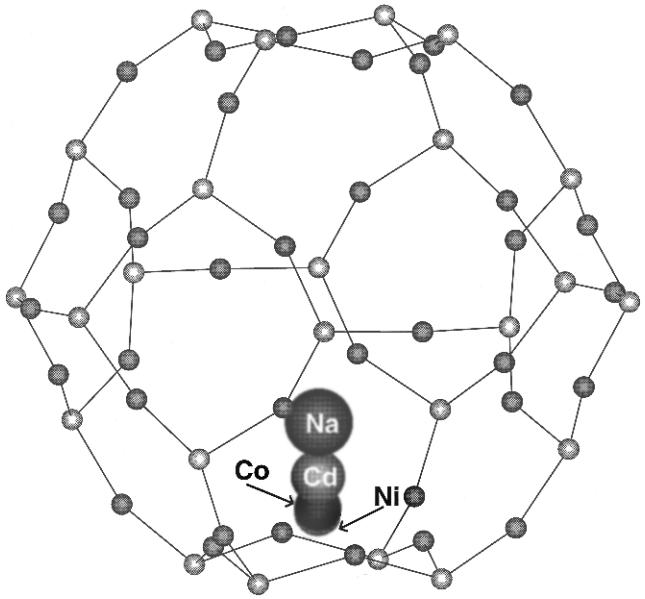

Figure 4. 4R′ adsorption site: a representation of the positions of the smaller cations tested, inside the sodalite unit located near the face of a four-ring window.

who identified the S6R adsorption site to be the most stable for sodium and found that cesium favors the S8R site only slightly over the S6R site. Thus, for the siliceous structure the overall finding is that the S8R adsorption site is preferred by the larger cations with ionic radii of >1 Å (Cs^+, K^+, Ba^{2+}, and Sr^{2+}). The cations with an ionic radius of <1 Å prefer the S6R adsorption site inside the α-cage as a consequence of the large relaxation of the silicon and oxygen ions in the six-ring. Calcium, with an ionic radius of 1 Å, is equally stable in the S6R and S8R sites and is only metastable in the S6R′ site. The sodium cation behaves like a cation with an ionic radius of <1 Å because it clearly prefers the S6R and 4R′ adsorption sites and therefore does not show the same behavior as calcium although it has an almost identical ionic radius. These results suggest that the stability of the cations in the identified adsorption positions is primarily driven by their ion size with a critical radius of 1 Å and relaxation of the framework.

As the experimental results were obtained from aluminated zeolite A, the next step was to study the effect of framework alumination on the cation adsorption positions.

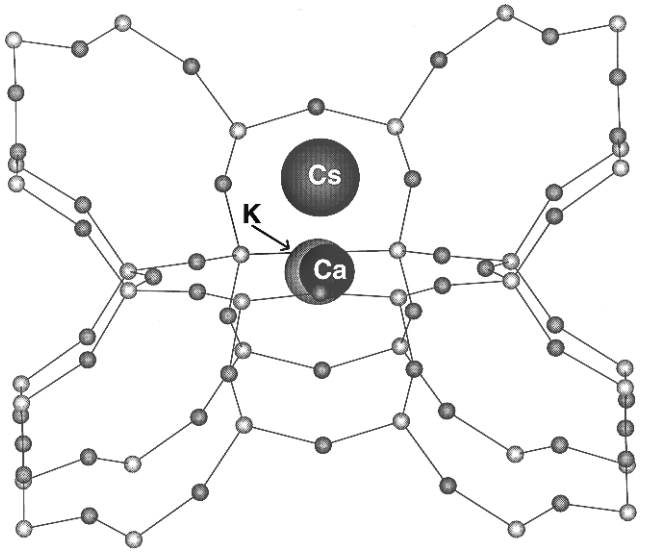

Figure 5. S8R adsorption site showing the three distinct cation positions found, where the calcium location is typical for all the cations studied with the exception of cesium and potassium.

5. Cation Exchange and Adsorption in Ca Na-A and Ca_5Na_2-A

5.1. Generation of the Bulk Structures. Fifty percent of the silicon atoms in the zeolite lattice were replaced by aluminum, and the net negative charge of this framework was compensated by a mixture of sodium and calcium cations. As there are no Al−O−Al bonds in the zeolite framework (Loewenstein's Rule),[50] the framework was simple to model, but locating the explicit site occupations of the charge-compensating cations was more complicated.

The neutron diffraction data of Haselden and Adams[47] identified a Ca/Na ratio of 2.5 ($Ca_{10}Na_4Si_{24}Al_{24}O_{96} = Ca_5Na_2$-A). This cation ratio creates two vacant adsorption sites per full unit cell. In addition, neutron diffraction identifies average site occupancies, whereas we considered explicit site occupations in the simulations. Therefore, as a way of accessing the importance of the cation distribution we have studied two Ca/Na distributions: (1) the CaNa-A structure ($Ca_8Na_8Si_{24}Al_{24}O_{96}$) where all the available adsorption sites are occupied and (2) the Ca_5Na_2-A structure.

The CaNa-A Structure. A number of Ca/Na distributions were investigated, and we found that the distribution with alternate calcium and sodium occupations produced a set of symmetric lattice vectors ($a = 24.67$ Å) and a lattice energy of −5421.9 eV, which was 0.76 eV more stable than the next lowest energy configuration calculated, indicating that we found a highly favorable CaNa-A structure. The volume of the CaNa-A structure increased by 12.85% compared to that of the relaxed siliceous structure and is just 0.25% larger than the crystallographic Ca_5Na_2-A structure analyzed by Adams and Haselden.[47]

The positions of both calcium and sodium were found to relax to the S6R sites inside the α-cage, even when the calcium ions were started in the S6R′ site. Subramanian and Seff[51] found in a crystallographic study of a dehydrated Ca_6-A structure that the calcium sites were located near the six-ring window with the main occupancy inside the α-cage (S6R) and a smaller occupation of the S6R′ site in the β-cage, while a sixth calcium atom was located in the center of an eight-ring window (S8R). Their result suggests that between the S6R and S6R′ sites, the S6R position is the more stable adsorption site for calcium in the zeolite A framework, which is in agreement with our calculations. Adams and Haselden[47] located the sodium ions in the S6R sites with calcium occupying the S6R′ sites inside the sodalite unit. The minimization simulation will not allow

the ions to pass energy barriers, and our result indicates that there is no barrier for calcium to travel from the S6R′ through a six-ring window to the S6R site. Furthermore, we did identify both the S6R and S6R′ sites to be adsorption sites for calcium in the purely siliceous zeolite, except that the S6R site was favored over the S6R′ site (see previous section 4.2). Further studies into the cation stability in additional adsorption sites will be discussed in section 5.2.

The Ca_5Na_2-A Structure. The stable cation configuration of the Ca_5Na_2-A structure was obtained by using a Monte Carlo approach to randomly select the cation positions from the available adsorption coordinates and then calculate its lattice energy. Approximately 3000 configurations were generated, but we only describe the simulation results on the most stable configuration. The minimized Ca_5Na_2-A structure showed a slight asymmetry ($a = 24.75$ Å), which is due to the irregular distribution of the two cation species (compared to the highly symmetric CaNa-A configuration). The unit cell of this Ca_5Na_2-A structure has expanded by 14.06% compared to the relaxed siliceous zeolite structure and is 1.22% larger than the crystallographic structure analyzed by Haselden and Adams.[47] On comparison to the relaxed CaNa-A structure, the Ca_5Na_2-A structure has increased in volume by 0.98%.

As in CaNa-A the calcium cations preferred to be located such that many of their nearest-neighbor cations were sodium ions. Both sodium and calcium ions were located inside the α-cages near the six-ring windows (S6R sites), as found in the stable CaNa-A configuration and found in experiment.[51] Additionally, the bond distances are in good accord with experiment; see, for example, the Na−O distances shown in Table 7, section 5.2.[9,47]

5.2. Cation Exchange: Comparison with Experiment. The previous section shows that the inclusion of aluminum resulted in the expansion of the zeolite framework, which had the effect of enhancing the sodium and calcium stability in their S6R adsorption sites, so much so that these sites near the six-rings inside the α-cage now became the most stable adsorption sites for calcium (compared to the siliceous form where calcium equally favored the S8R to the S6R adsorption site). Therefore we needed to study the effect of aluminum addition on the stability and the positions of the other exchangeable cations.

We found that the alumination of the zeolite lattice had a profound effect both on the cation positions as well as on the cation stability. Significantly, the results of both the CaNa-A and Ca_5Na_2-A structures were similar (i.e., the cations were in the same locations inside the α-cage), indicating that the difference in the cation distribution was not critical to the optimum cation positions and their stability in these adsorption sites.

Cation exchange was explored in the CaNa-A and Ca_5Na_2-A structures by removing either a single sodium or calcium ion and replacing it by another cation. The three adsorption sites identified in the siliceous structure (S8R, S6R, and the sodalite unit) and an additional site, which was found in the α-cage above a four-ring (4R), were probed for cation stability.

The ion-exchange results, when converted to solution energies, show that it is energetically more favorable, for example, to remove a calcium ion and replace it with two sodium ions than vice versa; i.e., we found it is energetically more favorable to produce CaNa-A than Ca_5Na_2-A. However, to avoid problems associated with the definition of solution energies, we present the results for the substitution of sodium by cesium and potassium and of calcium by other divalent cations, where the cation (either sodium or calcium) is removed from its most stable site (i.e., largest defect energy), and the energy of the metal oxide is obtained by minimizing the structure in PARAPOCS[16] using the potentials described in Table 1b, section I (for the metal oxide energies, see Table 5). Examples of the energy conversion of the calculated defect energy into solution energy are as follows:

TABLE 5: Calculated Lattice Energies of the Relaxed Metal Oxide Structures

metal oxide	minimized energy (eV)
BaO	−31.227
SrO	−32.496
CaO	−35.950
CdO	−36.703
NiO	−41.685
CoO	−40.916
Cs_2O	−20.337
K_2O	−25.301
Na_2O	−28.579

monovalent: $^1/_2Cs_2O + Na_{ZA} \rightarrow {}^1/_2Na_2O + Cs_{ZA}$

for SiO_2; $Na^+(S6R) \rightarrow Cs^+(S8R)$

$$^1/_2(-20.34) + (-4.01) \rightarrow {}^1/_2(-28.58) + (-2.67) = -2.78 \text{ eV}$$

for CaNa-A; $Na^+(S6R) \rightarrow Cs^+(S8R)$

$$^1/_2(-20.34) \rightarrow {}^1/_2(-28.58) + 2.62 = -1.50 \text{ eV}$$

divalent: $BaO + Ca_{ZA} \rightarrow CaO + Ba_{ZA}$

for SiO_2; $Ca^{2+}(S6R/S8R) \rightarrow Ba^{2+}(S8R)$

$$(-31.23) + (-10.64) \rightarrow (-35.95) + (-9.36) = -3.43 \text{ eV}$$

for CaNa-A; $Ca^{2+}(S6R) \rightarrow Ba^{2+}(S6R)$

$$(-31.23) \rightarrow (-35.95) + 3.68 = -1.04 \text{ eV}$$

The results comparing the solution energies of the exchanged cations for the three zeolite A structures are shown in Table 6. These show that the addition of aluminum has a profound effect on the stability and positions of the cations in the studied adsorption sites. However, the sodium and calcium distribution does not have a significant effect as the cations have similar solution energies in CaNa-A and Ca_5Na_2-A. Furthermore, the results show that after the addition of aluminum to the lattice all the studied cations are most stable at the S6R adsorption site inside the α-cage, with the exception of cesium, which is still more stable in the S8R adsorption site. The crystallographic results by Heo et al.,[10] Ahn and Iton,[49] Subramanian and Seff,[51] and Vance and Seff[9] all identified the S8R adsorption site to be the favorable position for cesium, with the S6R adsorption site being slightly less stable, thus supporting our calculated results. Moreover, the calculations for barium, which is another large cation, now show a clear preference for the S6R site, Where barium is located inside the α-cage at 0.90 Å from the six-ring window compared to 0.95 Å found experimentally in a dehydrated $Ba_{3.5}Na_5$-A structure.[52] The Ba−O distances with the six-ring oxygens are tabulated in Table 7, which also agree with experiment.[52]

The large cations (Cs^+, K^+, Ba^{2+}, and Sr^{2+}) also have a metastable site inside the sodalite cage near the six-ring window (S6R′). This is in contrast to the smaller cations (Cd^{2+}, Ni^{2+},

TABLE 6: Calculated Solution Energies of the Studied Exchangeable Cations[a]

	solution energy (eV)								
		CaNa-A				Ca_5Na_2-A			
cation	siliceous S6R*/S8R	S6R	S8R	S6R′/4R′	4R	S6R	S8R	S6R′/4R′	4R
barium	−3.43	−1.04	2.42	−0.29	NS	−1.10	1.88	−0.35	NS
strontium	−2.60	−0.74	3.38	NS[b]	NS	−0.77		1.42	NS
cadmium	0.32*	−0.47	6.06	NS	7.92	−0.46			7.94
nickel	2.23*	1.99	8.88	NS	9.62	2.04			9.57
cobalt	1.89*	1.68	8.92	NS	9.42	1.73			9.37
cesium	−2.78	−1.36	−1.50	−0.66	NS	−1.37	−1.51	−0.86	NS
potassium	−1.37	−0.55	0.54	NS		−0.54	0.35	−0.30	1.45

[a] The solution energies were calculated in relation to either sodium (in the case of the monovalent cations) or calcium (in the case of the divalent cations). In the case of the siliceous study, the cations are in infinite dilution. [b] NS = not stable.

TABLE 7: Cation−Oxygen Distances (in angstroms) in the Three Dehydrated Zeolite A Structures Compared to Experiment

cation	siliceous		aluminated		experiment	
S6R/S8R*	O(2)	O(3)	O(2)	O(3)	O(2)	O(3)
barium	2.91 (3)	2.66 (3)	3.14 (3)	2.57 (3)		2.51[52]
sodium	2.77 (3)	2.36 (3)	2.93 (3)	2.29 (3)	2.92[47]; 3.00[9]	2.37[47]; 2.22[9]
calcium	2.76 (3)	2.42 (3)	2.82 (3)	2.30 (3)	2.85[47]	2.29[47]
cadmium	2.57 (3)	2.35 (3)	2.77 (3)	2.27 (3)		2.27[11]

	O(1)	O(2)	O(1)	(O2)	O(1)	O(2)
cesium*	3.88 (4)	4.01 (4)	3.43 (2); 3.45; 3.46	3.60; 3.66 (2); 3.67	3.37[9]	3.43[9]

and Co^{2+}), which were stabilized in the 4R positions, their positive solution energies showing that their exchange with calcium to the 4R adsorption site is not energetically favorable. These metastable sites could become important adsorption sites at higher and/or mixed cation loading.[48,49,51,53]

The positive solution energies for cobalt and nickel suggest that zeolite A has a low selectivity for these cations. This is confirmed by Heo et al.,[54] who report that zeolite A has a low selectivity for cobalt, nickel, iron(II), and copper and that, with the addition of water, they can cause crystal damage due to hydrolysis of the framework. As shown by the low adsorption sites, in zeolite A the six-rings are too large for nickel and cobalt to form stabilizing cation−oxygen bonds, while the four-rings are too small. Considering these results we suggest that these small cations may favor cation exchange in zeolites that consist of five-rings (e.g., Clinoptilolite) and/or have a Si/Al ratio of >1 as the effect of aluminum addition is an expansion of the zeolite framework, including the ring sizes, and would be worthy of further investigation.

The addition of aluminum to the zeolite lattice caused the cadmium ions to become more stable in their S6R positions; the positive solution energy in the siliceous structure changed to negative solution energies in both CaNa-A and Ca_5Na_2-A means that exchanging these structures with cadmium would be energy driven. This is in agreement with Jang et al.,[11] who prepared a dehydrated Cd_6-A structure, where four cadmium ions were located inside the sodalite unit along the [111] direction at a distance of 0.50 Å from the hexagonal window, bound to three of its oxygens (S6R′). The other two cadmium ions extended 0.28 Å into the large cavity in their S6R positions. Although our results thus far have not found the S6R′ adsorption site in the aluminated structures, our S6R adsorption site is 0.21 Å extended from the hexagonal windows (with Cd−O(3) = 2.27 Å(3) and Cd−O(2) = 2.77 Å(3); see also Table 7)). In zeolites with a higher Si/Al ratio cadmium could prefer the S8R adsorption site[55] because the oxygen atoms would be closer to the cation occupying this S8R site, as from simple geometric considerations the eight-ring will be of an oval shape instead of the circular shape in the zeolite A structure, because Si−O and Al−O have different bond lengths.

In general, the S6R adsorption sites for CaNa-A and Ca_5Na_2-A were found closer to the plane of the six-ring than the adsorption sites in the siliceous structure e.g. 1.55 Å (aluminated) versus 2.13 Å (siliceous) for cesium, and 0.90 Å (aluminated) versus 1.38 Å (siliceous) for barium. In addition, the cation−O(3) distances were reduced, while the cation−O(2) distances were increased due to the addition of aluminum to the lattice; see Table 7 for some examples.

The adsorption sites in the eight-rings also changed on aluminum addition with the exception of cesium. All the other cations moved off-center toward the wall of the eight-ring, (although still in plane), because the addition of aluminum to the zeolite framework caused the eight-ring to expand (Al−O bonds are longer than Si−O bonds). This forced the cations to move off-center to reduce their distance with two of the ring oxygens to form stabilizing bonds rather than no bonds. The cation off-center position in the plane of the eight-ring has been identified previously in experiment, i.e., for potassium[7,8,48] and barium.[52] In contrast, the cesium ion was still centered in front of the eight-ring window even though it did move closer to the eight-ring window, which reduced its distance to all eight oxygens, compared to the S8R position in the siliceous structure (see Table 7). These Cs−O distances we found were larger than quoted by Vance and Seff[9] (see Table 7). This difference is probably due to the cesium potential overestimating the repulsive forces but could be due to other factors that might decrease the Cs−O distances, such as thermal effects or the presence of water. For a Cs_{12}-A structure, Subramanian and Seff[51] and Ahn and Iton[49] quoted that, per unit cell, there are three available sites in the eight-ring windows and eight near the six-ring windows, either inside the α-cage or inside the sodalite units. A 12th site is located inside the α-cage above a four-ring window. We found this 12th site (4R) to be unstable for cesium; perhaps it needs to be stabilized by the formation of cesium clusters or by the presence of some surrounding water molecules. This would explain why the 4R site is found experimentally at higher cesium concentrations. Our results suggest that the S8R adsorption sites will be occupied first as they are the most stable sites for cesium.

In summary, the effect of aluminum addition to the zeolite framework causes the ring structures to expand, and this increases the bond lengths between the extraframework cation and the oxygens in the ring, which reduces stability. Additionally, the presence of aluminum in the zeolite framework reduces the repulsive forces between the framework silicons and the exchangeable cation, due to the effective negative charge of the aluminum atoms. The combination of these two effects could explain why the cation distances from the six-ring windows and the cesium distance to the eight-ring window reduce and why all the other cations move closer to the wall of the eight-rings. In addition, it might explain why all the cations

TABLE 8: Relative Stability of Calcium and Strontium Ions in the Six- and Eight-Ring for Two Potential Models[a]

	relative stability (eV)		
	siliceous		
cation	rigid	relaxed	CaNa-A relaxed
$Sr^{2+}(1)$	+2.8	+0.9	−4.1
$Sr^{2+}(2)$	+2.5	+1.0	−4.5
$Ca^{2+}(1)$	+1.7	0.0	−5.6
$Ca^{2+}(2)$	+0.9	−1.9	−6.2

[a] A negative value indicates that the six-ring is the most stable adsorption site, while a positive value indicates that the eight-ring site is favored.

favor the S6R adsorption sites over the S8R adsorption sites, since there are three stabilizing cation−oxygen bonds possible with the six-ring oxygens compared to just two with the eight-ring oxygens, except for cesium, which can still form four stabilizing bonds with the eight-ring oxygens.

6. Potential Sensitivity

When two potential models, which have been derived independently, satisfy our criteria, as is the case for strontium, we can use this to estimate the magnitude of the uncertainty in the defect energies. This is shown in Table 8. The relative stability of calcium and strontium in the six- and eight-ring sites is tabulated for the two different potential models used. A negative value indicates the preference of the cation for the six-ring site, whereas a positive value means that the cation is most stable in the eight-ring position. The calcium results are shown because the zeolite simulation results show a sensitivity toward the two calcium potentials used. In the siliceous zeolite structure, the Ca(1) ion equally favors the S6R to the S8R adsorption site, while the Ca(2) has a smaller effective radius and therefore clearly prefers the S6R adsorption site. The Ca-(2) potential model produces elastic constants that are stiffer than experimentally found for calcium silicates (see Table 2b).[28] The Ca(1) potential, although not perfect, produces a calcium ion that is the right size and has been found to satisfy our criteria better that the Ca(2) potential. However, the small change in effective radius causes a change in adsorption site stability in the siliceous zeolite A structure, indicating a sensitivity in site stability that is ion size dependent. This illustrates that care must be taken in selecting the interatomic potentials and in specific calculations the results obtained with different potentials, such as calcium, should be compared, e.g., when simulating the effect of hydration.

7. Activation Energies for Diffusion

The activation energies for sodium, calcium, and cesium in siliceous zeolite A were calculated to make an initial study of their diffusion pathways through the framework. The activation energy is the energy required for a cation to leave one stable adsorption site for another and can be determined from saddle point energies.

The saddle points for all three cations were identified between the six-ring and eight-ring windows perpendicular to the shared oxygen atom, with cation−oxygen distances of 2.55 Å for sodium and calcium and 2.89 Å for cesium. The activation energies are as follows: 1.52 eV (S6R → S8R) and 1.54 eV (S8R → S6R) for calcium, 0.83 eV (S6R → S8R) and 0.61 eV (S8R → S6R) for sodium, and 0.67 eV (S6R → S8R) and 0.81 eV (S8R → S6R) for cesium. Therefore despite the difference in size we predict that cesium and sodium have similar energetic barriers to migration. As the location of the energy barriers was close to the wall at the intersection of the six- and eight-ring, the cations will travel close to the walls of the large cavities when migrating through the zeolite, as predicted for the hydrocarbons.[56]

8. Summary and Conclusions

We have used atomic simulation techniques to model ion-exchange behavior in three dehydrated zeolite A structures. From the results of these calculations we can make the following observations:

Framework relaxation is a very important component in the interaction between cation and framework, and the zeolite lattice cannot be viewed as a rigid structure through which atoms move as has been used in earlier simulations. The cation adsorption sites located in the three relaxed structures (siliceous, CaNa-A, and Ca_5Na_2-A) were found to agree very well with experimental data, and these adsorption sites are the following: (i) the S8R site in the plane of the eight-ring windows, (ii) the S6R site located along the [111] direction toward the plane of the six-ring windows inside the large α-cage, (iii) the 4R site inside the large α-cage, near the center of the four-rings, and in the sodalite unit, (iv) for the larger cations studied (ionic radius > 1 Å), near the face of the hexagonal windows along the [111] direction (S6R′ site) and for the smaller cations studied, the 4R′ site above the four-rings. Some recent experiments[48,49,51,53] have indicated that the metastable adsorption sites identified in this work could become important adsorption sites at higher cation loading and when competing cationic species are introduced.

The effect of aluminum addition to the zeolite framework causes the ring structures to expand, increasing the bond lengths between the extraframework cation and the oxygens in the ring, which reduces the stability. If it were purely the electrostatic forces controlling the cation positions, the reduction of electrostatic repulsion due to aluminum addition would favor cations in the S8R site (four aluminum atoms per eight-ring), but this is not the case. A combination of both effects (expansion of the ring sizes and reduction of the repulsive forces) explains why the cation distances from the six-ring windows and the cesium distance to the eight-ring window reduce and why all the other cations move closer to the wall of the eight-rings. In addition, this result might explain why all the cations favor the S6R adsorption sites over the S8R adsorption sites, since there are three stabilizing cation−oxygen bonds possible with the six-ring oxygens compared to just two with the eight-ring oxygens, except for cesium, which can still form four stabilizing bonds with the eight-ring oxygens.

With the exception of nickel and cobalt, all the exchangeable cations studied will sorb into the zeolite structures (CaNa-A and Ca_5Na_2-A) in favor of sodium and calcium. In addition, our calculations showed that it is energetically more favorable to load the zeolite with sodium than with calcium.

The initial results of our study into cation diffusion indicates that the cations travel close to the walls of the large cavity when migrating through the zeolite. These results indicate agreement with our adsorption and ion-exchange results where the ability to form bonds with lattice oxygens is a key factor to the cation site stability. Future simulations will include more detailed studies into cation diffusion. However, the main focus in future simulations will be the effect of water[57] on the adsorption and ion-exchange behavior of cations in zeolites, as experiments have identified its importance, e.g., its stabilizing (barium-exchanged zeolite A)[52] and destabilizing effect (nickel, cobalt, iron(II), or copper-exchanged zeolite A).[54,58] The latter effect is possibly due to cation hydrolysis, which leads to substantial proton concentrations within the zeolite, causing destruction of the zeolite framework.[54,58]

Acknowledgment. We would like to thank EPSRC for the provision of a studentship, NERC for the provision of the computing facility, and MSI for the provision of Insight II.

References and Notes

(1) Fergusson, J. E. *The Heavy Elements: Chemistry, Environmental Impact and Health Effects*: Pergamon Press plc: Oxford, 1991; Chapter 1.
(2) Ames, Jr. L. L. *Am. Miner.* **1960**, *45*, 689.
(3) Kesraoui-Ouki, S.; Cheeseman, C. R.; Perry, R. *J. Chem. Technol. Biotechnol.* **1994**, *59*, 121.
(4) Zamzow, M. J.; Murphy, J. E. *Sep. Sci. Technol.* **1992**, *27*, 1969.
(5) Dyer, A.; Aboujamous, J. K. *J. Radioanal. Nucl. Chem.−Art.* **1994**, *183*, 225.
(6) Sherman, J. D. *Am. Inst. Chem. Eng. Symp. Ser.* **1978**, *74*, 98.
(7) Leung, P. C. W.; Kunz, K. B.; Seff, K.; Maxwell, I. E. *J. Phys. Chem.* **1975**, *79*, 2157.
(8) Pluth, J. J.; Smith, J. V. *J. Phys. Chem.* **1979**, *83*, 741.
(9) Vance, jr. T. B.; Seff, K. *J. Phys. Chem.* **1975**, *79*, 2163.
(10) Heo, N. H.; Dejsupa, C.; Seff, K. *J. Phys. Chem.* **1987**, *91*, 3943.
(11) Jang, S. B.; Kim, U. S.; Kim, Y.; Seff, K. *J. Phys. Chem.* **1994**, *98*, 3796.
(12) Jackson, R. A.; Catlow, C. R. A. *Mol. Simul.* **1988**, *1*, 207.
(13) Jackson, R. A.; Bell, R. G.; Catlow, C. R. A. *Recent Advances in Zeolite Science*; In Klinowski, J., Barrie, P. J., Eds.; Studies in Surface Science and Catalysis 52; Elsevier: Amsterdam, 1989; p 203.
(14) Catlow, C. R. A., Ed.; *Modelling of Structure and Reactivity in Zeolites*: Academic Press Ltd.: London, 1992; Chapter 3.
(15) Born, M.; Huang, K. *Dynamical Theory of Crystal Lattices*; Oxford University Press: Oxford, 1954.
(16) Parker, C. S.; Price, G. D. *Adv. Solid State Chem.* **1989**, *1*, 295.
(17) Leslie, M. SERC Daresbury Report DL/SCI/TM31T; CRC: Daresbury; 1982.
(18) Mott, N. F.; Littleton, M. J. *Trans. Faraday Soc.* **1938**, *34*, 485.
(19) Stoneham, A. M.; Harding, J. H. *Annu. Rev. Phys. Chem.* **1986**, *37*, 53.
(20) Cherry, M.; Islam, M. S.; Catlow, C. R. A. *J. Solid State Chem.* **1995**, *118*, 125.
(21) Islam, M. S.; Winch, L. J. *Phys. Rev. B: Condens. Mater.* **1995**, *52*, 10510.
(22) Harding, J. H. *Water Chemistry of Nuclear Reactor Systems 7*; BNES: London, 1996; Vol. 1, p 309.
(23) Lewis, G. V.; Catlow, C. R. A. *J. Phys. Chem. Solid State Phys.* **1985**, *18*, 1149.
(24) Gale, J. D. *Philos. Mag. B* **1996**, *73*, 3.
(25) Dick, B. G.; Overhauser, A. W. *Phys. Rev. B* **1958**, *112*, 90.
(26) Colbourn, E. A. *Surf. Sci. Rep.* **1992**, *15*, 281.
(27) Sanders, M. J.; Leslie, M.; Catlow, C. R. A. *J. Chem. Soc., Chem. Commun.* **1984**, 1271.
(28) Watson, G. W. Ph.D. Thesis, University of Bath, 1994.
(29) De Boer, K.; Jansen, A. P. J.; van Santen, R. A.; Watson, G. W.; Parker, S. C. *Phys. Rev. B* **1996**, *54*, 826.
(30) James, R. *D.* Philos. Thesis, Oxford University, 1979.
(31) Post, J. E.; Burnham, C. W. *Am. Miner.* **1986**, *71*, 142.
(32) Parker, S. C. Ph.D. Thesis, University of London, 1983.
(33) Catlow, C. R. A. *Proc. R. Soc. London A* **1977**, *353*, 533.
(34) Purton, J.; Catlow, C. R. A. *Am. Miner.* **1990**, *75*, 1268.
(35) Gordon, R. G.; Kim, Y. S. *J. Chem. Phys.* **1972**, *56*, 3122.
(36) Lepage, Y.; Calvert, L. D.; Gabe, E. J. *J. Phys. C: Solid State Phys.* **1980**, *41*, 721.
(37) Harlow, G. E.; Brown, G. E. *Am. Miner.* **1980**, *65*, 986.
(38) Levien, L.; Prewitt, C. T. *Am. Miner.* **1981**, *66*, 315.
(39) Deer, W. A.; Howie, R. A.; Zuessman, J. *An Introduction to the Rock Forming Minerals*; Longman Group Ltd.: U.K., 1982.
(40) McSkimin, H. J.; Andreatch, P.; Thurston, R. N. *J. Appl. Phys.* **1965**, *36*, 1624.
(41) Suzuki, I.; Anderson, O. L.; Sumino, Y. *Phys. Chem. Miner.* **1983**, *10*, 38.
(42) Levien, L.; Weidner, D. J.; Prewitt C. T. *Phys. Chem. Miner.* **1978**, *4*, 105.
(43) Meier, W. M.; Olson, D. H.; Bearlocher, Ch. *Atlas of the Zeolite Structure Types*; Elsevier: London, 1996; p 31.
(44) Barrer, R. M. *Zeolites and Clay Minerals as Sorbents and Molecular Sieves*; Academic Press: London, 1978; Chapter 2.
(45) Beagley, B.; Titiloye, J. O. *Struct. Chem.* **1992**, *3*, 429.
(46) Breck, D. W. *Zeolite Molecular Sieves*; John Wiley and Sons, Inc.: New York, 1974.
(47) Adams, J. M.; Haselden, D. A. *J. Solid State Chem.* **1984**, *51*, 83.
(48) Armstrong, A. R.; Anderson, P. A.; Edwards, P. P. *J. Solid State Chem.* **1994**, *111*, 178.
(49) Ahn, M. K.; Iton, L. E. *J. Phys. Chem.* **1991**, *95*, 4496.
(50) Loewenstein, W. *Am. Miner.* **1954**, *39*, 92.
(51) Subramanian, V.; Seff, K. *J. Phys. Chem.* **1980**, *84*, 2928.
(52) Kim, Y., Subramanian, V., Firor, R. L., Seff, K. In *Adsorption and Ion Exchange with Synthetic Zeolites*; Flank, W. H., Ed.; ACS Symposium Series 135; American Chemical Society: Washington, DC, 1980, Chapter 7.
(53) Armstrong, A. R.; Anderson, P. A.; Edwards, P. P. *J. Phys. Chem.* **1994**, *98*, 9279.
(54) Heo, N. H.; Cruz-Patalinghug, W.; Seff, K. *J. Phys. Chem.* **1986**, *90*, 3931.
(55) Parise, J. B.; Liu, X.; Corbin, D. R. *J. Chem. Soc., Chem. Commun.* **1991**, *3*, 162.
(56) Barrer, R. M. *Zeolites and Clay Minerals as Sorbents and Molecular Sieves*; Academic Press: London, 1978; Chapter 6.
(57) Smith, L.; Cheetham, A. K.; Morris, R. E.; Marchese, L.; Thomas, J. M.; Wright, P. A.; Chen, J. *Science* **1996**, *271*, 799.
(58) Dooryhee, E.; Catlow, C. R. A.; Couves, J. W.; Maddox, P. J.; Thomas, J. M.; Greaves, G. N.; Steel, A. T.; Townsend, R. P. *J. Phys. Chem.* **1991**, *95*, 4514.